Journal of Nuclear Materials 409 (2011) 33–39

Contents lists available at ScienceDirect

Journal of Nuclear Materials

journal homepage: www.elsevier.com/locate/jnucmat

Framework model for hydrogen redistribution in Zircaloy sheathing

G. Bruni [1], B.J. Lewis *, W.T. Thompson

Royal Military College, Department of Chemistry and Chemical Engineering, PO Box 17000 Kingston, Ontario, Canada K7K 7B4

ARTICLE INFO

Article history:
Received 3 October 2010
Accepted 10 December 2010
Available online 21 December 2010

ABSTRACT

Models have been developed to describe secondary hydriding phenomena. Thermodynamic models for the Zr–H and Zr–O–H systems provide the terminal solubility of dissolved hydrogen and oxygen in the α-Zr phase as a function of temperature and partial pressure. A simulation of the Sawatzky and Vogt experiment, based on a finite-element kinetic model with the thermodynamic predictions as a boundary condition, is further developed to describe the redistribution of hydrogen in a Zircaloy-2 sample placed in a temperature gradient. This analysis confirms the hydrogen diffusion coefficient.

Crown Copyright © 2010 Published by Elsevier B.V. All rights reserved.

1. Introduction

With the occurrence of a defective fuel element, coolant can enter into the fuel-to-sheath gap. The coolant that flashes to steam in the gap (due to higher temperatures near the fuel) may oxidize the fuel and any areas of the inner layer of the sheath not covered by ZrO_2. These reactions, in addition to H_2O (or D_2O) radiolysis, lead to hydrogen (deuterium) production in the gap. A sufficient build up of hydrogen (deuterium) in the gap (i.e. a critical H_2/H_2O or D_2/D_2O ratio), usually at locations far away from the defect, can lead to sheath hydriding (deuteriding) [1–9]. The hydriding process occurs through the following reaction (in the following analysis only H_2 and H_2O are considered although a similar analysis can be considered for the heavy water system):

$$H_2(g) + Zr(\alpha) \rightarrow ZrH_2(\delta) \quad (1)$$

Hydrogen diffusion through ZrO_2 is very slow and, therefore, hydriding is only likely to occur on a bare area of the sheath or where the protective oxide has broken down. This exposure may result from sheath thermal expansion and ZrO_2 cracking during online refueling processes in the CANDU reactor. The molar volume of the δ-hydride phase is 17% greater than that of the original phase of zirconium (α-Zr) in the sheath [10]. A hydride blister eventually grows in the "sunburst" shape shown in figures (A) and (B). The increases in molar volume of the sheath make it brittle and can lead to secondary defects (figure (B)) with associated fission product release.

2. Thermodynamic modelling of the Zr, H and O system

Both the Zr–H binary and Zr–O–H ternary systems were modelled using Gibbs energy minimization calculations. The complete details of this treatment are presented in Ref. [11]. These calculations determine the phase, or combination of phases, that has the lowest Gibbs energy and is the most favourable to form thermodynamically. The Gibbs energy of a phase (Fig. 2) can be divided into contributions from each of the m components that make up the phase ϕ, described by the partial molar Gibbs energy property (G) in Fig. 2. This property for each component i at a temperature T involves: (i) a reference Gibbs energy ($G_i^{0,REF}$) defined by the standard enthalpy (ΔH_f^0), absolute entropy (S^0) and molar capacity (c_p) and (ii) the contribution to the Gibbs energy of mixing ($\Delta \bar{G}_{MIX,i}^{\phi}$) given by an ideal partial mixing term ($\Delta \bar{G}_i^{I,\phi}$) and excess partial mixing term ($\Delta \bar{G}_i^{E,\phi}$) (a term used to provide a faithful fit to experimental data). Here X is the mole fraction for component i in a given phase.

The Zr–H binary system modelling was based on the experimental data of the Bulletin of Alloy Phase Diagrams (BAPD) which included experimental information on H_2 partial pressures incorporated in the current thermodynamic model [12]. The partial molar Gibbs energies are provided for each component in Table 1. Note that these properties are only valid for temperatures up to 550 °C.

The above table shows the component selection for each of the phases modelled. Components are the formal way of specifying the composition of a phase. The selection is best made so as to minimize the need for an excess term. The components of Zr and ZrH were chosen for the α-Zr phase since hydrogen is a very small atom in relation to the Zr atom and has a high affinity for zirconium. This selection respects Sievert's Law which states that H_2 gas dissociates on the surface of α-Zr and enters the metal as atomic hydrogen [13]. The Zr–H model is shown in Fig. 3 which includes calculated

* Corresponding author. Tel.: +1 613 541 6611; fax: +1 613 542 9489.
E-mail address: lewis-b@rmc.ca (B.J. Lewis).
[1] Present address: Oxford University, United Kingdom.

0022-3115/$ - see front matter Crown Copyright © 2010 Published by Elsevier B.V. All rights reserved.
doi:10.1016/j.jnucmat.2010.12.030

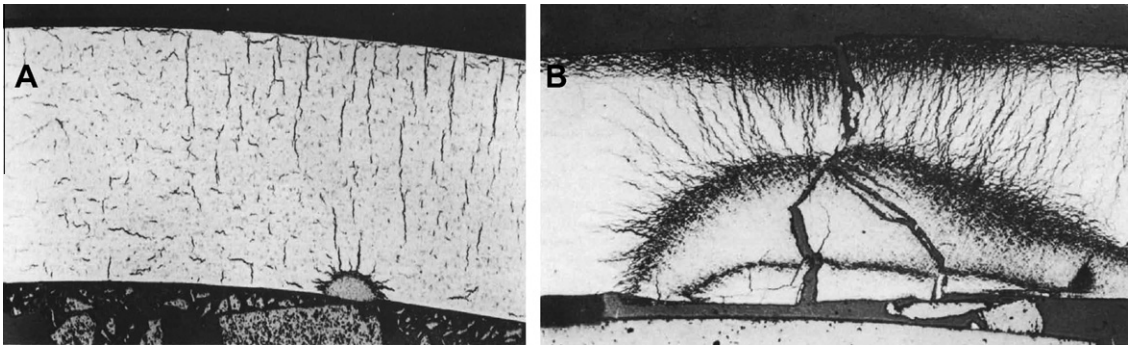

Fig. 1. (A) Early stage of sunburst formation in fuel sheath. (B) Crack propagation through sunburst hydride region [3].

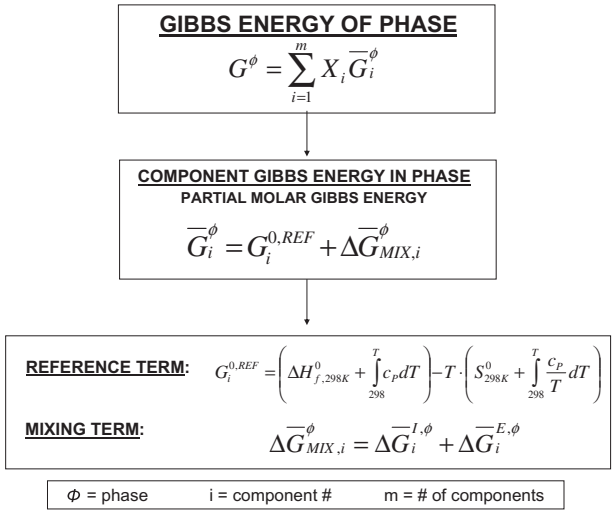

Fig. 2. Cornerstone equations to provide the Gibbs energy for an *m* component phase.

partial pressure H_2 isobars. The ZrH component is a fictive species introduced to fit the known data in Fig. 3. JANAF values are used for the H and H_2 gas species for the computation of the hydrogen gas partial pressures in Fig. 3 [11]. Table 1 also shows that only ideal mixing of these components is necessary, where no excess mixing parameters were required. The complete methodology for the modelling of the phase diagram by Gibbs Energy Minimization and component selection is detailed in Ref. [11].

This treatment specifically provides a computational means to reproduce the phase diagram quantitatively for a more general multi-component analysis (with the added ability to predict H_2 isobars, solubilities, etc.). Specific points along the α-Zr terminal solubility line (α/α + δ phase boundary) of the Zr–H binary system provide the critical boundary conditions for the kinetics model for sheath hydriding (Section 3). Fig. 4 shows good agreement between the Zr–H model (dotted) with experimental data of [12].

The Zr–O binary system was also modelled using Gibbs energy minimization techniques. The properties for the partial molar Gibbs energy for each component in each phase of the system are outlined in the subsequent two tables where *R* is the ideal gas constant.

The thermodynamic properties of Tables 2 and 3 provide the Zr–O model of Fig. 5, shown with respect to phase boundaries defined by the experimental data used to model the system below 1200 °C from Ref. [14]. A large negative excess Gibbs energy is required for O in the α-Zr phase to provide for the high O solubility as well as the very negative Gibbs energy of the formation of ZrO_2. For the current application, where the hydriding experiments of Swatzky in Section 3 are only conducted up to 750 K and for typical cladding temperatures which arise in normal operating fuel elements, it is not necessary to consider the non-stoichiometry of the ZrO_{2-x} phase that only becomes important above 1525 °C.

The Zr–O model is used in conjunction with the Zr–H model to give a Zr–O–H ternary system. The importance of including oxygen in the thermodynamic modelling of hydriding is evident from:

$$Zr + 2H_2O \leftrightarrow ZrO_2 + 2H_2 \quad (2)$$

At an approximate sheath inner layer temperature of 300 °C, the change in Gibbs energy for the reaction in Eq. (2) is ~ −1000 kJ mol^{-1} whereas the value for the zirconium hydriding reaction at the same temperature is only ~ −100 kJ mol^{-1} [15]. This shows that thermodynamically, sheath oxidation is largely favoured when zirconium is in contact with both oxygen and hydrogen. It is important to include oxygen in the analysis of the thermodynamics of hydriding phenomena.

The thermodynamic properties of Tables 1–3 were combined to develop the isothermal Zr–O–H ternary diagram illustrated in Fig. 6.

The α-Zr(O,H) phase field cannot be seen in Fig. 6 since the concentration of hydrogen is extremely low. The Zr corner of the ternary diagram is therefore expanded and placed on the plot in Fig. 7 to show these phase regions. Note that the at.% hydrogen on the *x*-axis is on a log scale and the equilateral triangle of Fig. 6 is replaced by a right scalene triangle in Fig. 7.

The critical partial pressure conditions required to form δ-hydride in the presence of water vapour (the conditions in the

Table 1
Thermodynamic properties of Zr–H binary system at and below 550 °C.

Phase	Component	$\Delta H^0_{f,298K}$ (J mol^{-1})	S^0_{298K} (J K^{-1} mol^{-1})	c_p (J K^{-1} mol^{-1})	$\Delta\overline{G}_i^{I,\phi}$ (J mol^{-1})	$\Delta\overline{G}_i^{E,\phi}$ (J mol^{-1})
α	Zr	0	38.87	25.20	$RT\ln X_{Zr}$	0
	ZrH	−55,220	51.27	43.80	$RT\ln X_{ZrH}$	0
δ	ZrH	−86,640	33.00	43.80	$RT\ln X_{ZrH}$	0
	ZrH_2	−172,800	35.04	30.95	$RT\ln X_{ZrH2}$	0
ε	ZrH_2	−184,300	32.62	30.95	$RT\ln X_{ZrH2}$	0

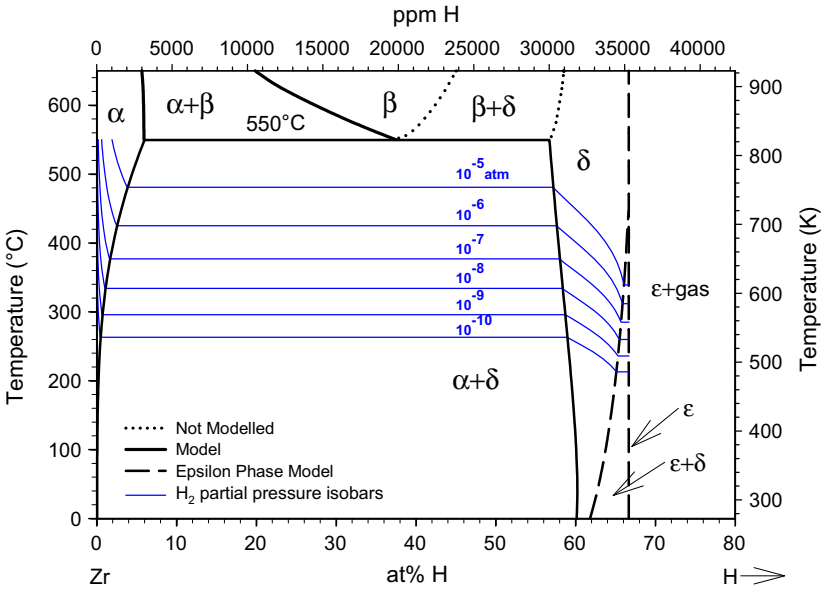

Fig. 3. Zr–H binary model with H_2 partial pressure isobars.

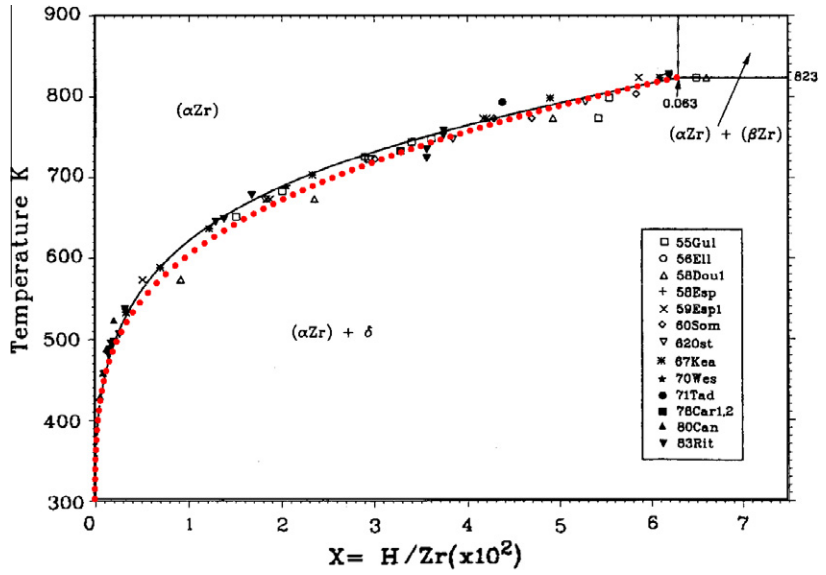

Fig. 4. Zr–H model superimposed (dotted) on experimental data of [12].

Table 2
Thermodynamic properties of Zr–O binary system.

Phase	Component	Reference component	$G_i^{0,Phase} - G_i^{0,REF}$ [a] (J mol^{-1})	$\Delta\overline{G}_i^{E,\phi}$ (J mol^{-1})	$\Delta\overline{G}_i^{E,\phi}$ (J mol^{-1})
α-Zr	Zr	Zr(α)	0	$RT\ln X_{Zr}$	$-523,730 \cdot 4(X_{Zr}^{\alpha})^3(X_O^{\alpha})^2$
α-Zr	O	O(g)	−773,170 + 155T	$RT\ln X_O$	$-523,730(-3X_{Zr}^{\alpha 4} + 4X_{Zr}^{\alpha 3})$
ZrO_2	ZrO_2	ZrO_2(s)	0	$RT\ln X_{ZrO_2}$	Stoichiometric, no mixing

[a] The relationship between O in the gas phase (reference state) and in the α-Zr phase (solution phase) can be represented by $O(g) \leftrightarrow O(\alpha)$ and $\Delta G_{O(g)\leftrightarrow O(\alpha)^0} = G_O^{0,\alpha} - G_O^{0,gas} = -773{,}170 + 155T$.

three phase region of Fig. 7) were determined using the ternary model and are outlined in Table 4.

Table 4 indicates that, in principle, a virtually pure hydrogen environment is required for hydriding to occur. This main conclusion, that the water vapour concentration must be very low for hydriding to pre-empt oxidation, resonates with the experimental results of numerous other researchers [16–19].

The thermodynamic models also provide significant information on the specific partial pressure of hydrogen required to form δ-hydride for a given temperature. This is of course dependent on the given atmospheric environment as illustrated in Table 5.

According to the proposed Zr–H binary model (Fig. 3), a partial pressure of 8.2×10^{-9} atm is required to hydride pure zirconium at 300 °C. When zirconium coexists with ZrO_2 in an oxidizing

Table 3
Reference properties of components in the Zr–O binary system.

Phase	Comp.	Ref. comp.	Reference properties		
			$\Delta H^0_{f,298\ K}$ (J mol^{-1})	$S^0_{298\ K}$ (J K^{-1} mol^{-1})	c_p (J K^{-1} mol^{-1})
α-Zr	Zr	Zr(α)	0	38.87	25.20
α-Zr	O	O(g)	249,170	160.95	$19.96 + 2.64 \times 10^{-4}T + 58654T^{-2} - 3.70 \times 10^{-8}T^2 + 20.95T^{-0.5}$
ZrO_2	ZrO_2	ZrO_2(s)	−10,97,460	50.35	$94.62 - 584.84\,T^{-0.5} - 1.204 \times 10^8\,T^{-3}$

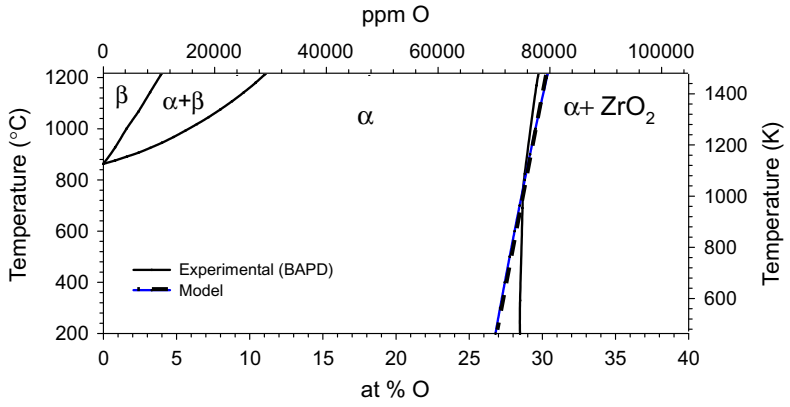

Fig. 5. Zr–O model shown with respect to BAPD experimental data [14].

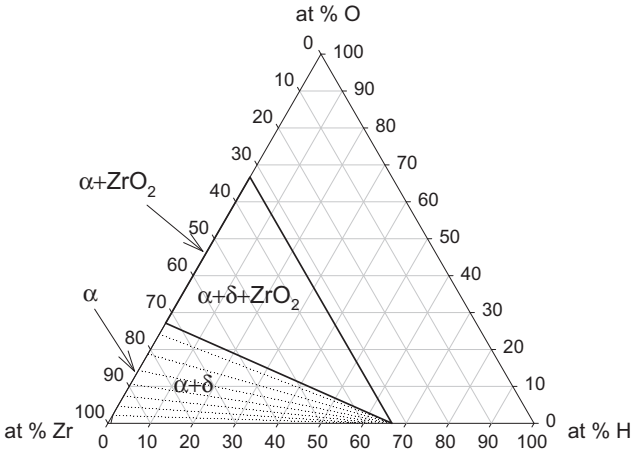

Fig. 6. Zr–O–H ternary diagram without ε-hydride phase (300 °C).

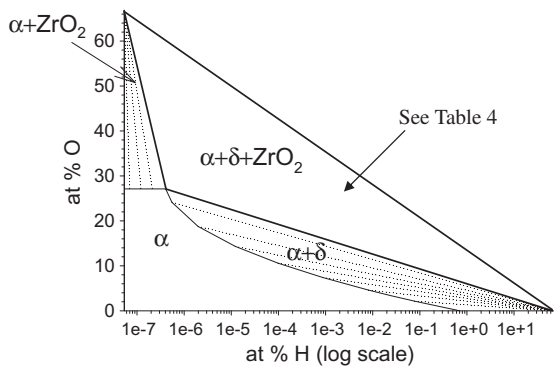

Fig. 7. Zr–O–H ternary diagram near Zr corner (300 °C).

Table 4
Critical partial pressure conditions to form δ-hydride in the presence of H_2O at 300 °C.

Zr–O–H ternary (δ-hydride, α-Zr and ZrO_2 coexist)
$P_{H_2} = 1 \times 10^{-3}$ atm $P_H = 2 \times 10^{-19}$ atm $P_{H_2O} = 3 \times 10^{-26}$ atm

Table 5
Partial pressures and activities for critical hydriding based on thermodynamic models.

Temperature (°C)	Environment (1 atm total pressure)	Thermodynamic model used	H_2 partial pressure required to hydride
330	Reducing, no H_2O	Zr–H Fig. 3	8.2×10^{-9} atm
330	Oxidizing (~10^{-24} atm H_2O)	Zr–O–H Fig. 7	6.2×10^{-2} atm

environment, the Zr–O binary model (Fig. 5) shows that a significant amount of hydrogen (in excess of 25 at.%) is dissolved in the metal. The model also implies that the activity of α-Zr and subsequently its capacity to acquire any hydrogen is reduced. This accounts for an increased partial pressure of 6.2×10^{-2} atm required to hydride zirconium (300 °C) in an environment with even minute quantities of water vapour.

The oxide layer will inhibit secondary hydriding. It is believed that only when this oxide layer is cracked or degraded that the hydrogen can dissolve directly into the Zr-based sheath. When the ZrO_2 forms on the surface of the sheath, it is in a state of high compression but adherent, and is therefore protective. The compressive stress is due to the larger specific volume of the ZrO_2. It is so compressed that the oxide on the surface of the sheath resembles a cubic structure and not a monoclinic one as predicted by the Zr–O binary equilibrium diagram of Fig. 5 [20].

3. Simulation of the Sawatzky and Vogt experiment

Since the early 1960s, the experiment performed by Sawatzky has been frequently cited in relation to the transient distribution of hydrogen in a Zircaloy-2 sample [21]. The experimental data were originally interpreted by Sawatzky and Vogt analytically [22,23]. The Sawatzky and Vogt analysis has been considered in other numerical treatments where the hydriding rate in the two-phase region is approximated by assuming an equilibrium between the solid solution and the terminal solid solubility with only diffusion in just the dominant component of the second phase [24,25]. In particular, these latter treatments are only valid for: (i) interstitial solutes and cases in which the second phase is not dominant, and the mobility of the solute is much greater than that of the solvent, and (ii) where there is local equilibrium in those regions in which the solubility limit is exceeded [24]. The current work involves a re-modelling of the experimental results [21] by finite-element numerical methods in COMSOL Multiphysics, accounting for the more rigorous treatment of Sawatzky and Vogt [22,23]. The complete details of this work are given in Ref. [11]. This approach does not require the mathematical simplifications involved in arriving at an analytical solution. The result of this model will confirm the diffusion coefficient of hydrogen in α-Zr.

In the Sawatzky experiment, a Zircaloy-2 sample was annealed in a hot hydrogen environment in order to initially provide a homogenous hydrogen profile [21]. The sample was then exposed to air in order to oxidize the outer sheath surface and prevent escape of hydrogen. The final result was a uniform distribution of δ-hydride in an H saturated α-Zr matrix. Next, a temperature gradient was applied by holding one end of the sample at a cold temperature and the other end at a hot temperature. The gradient is assumed to be linear. The sample was left at this condition for several weeks until post-experiment examination could be performed to measure the transient hydrogen distribution. Hydrogen concentrations in the final sample were measured in 0.1 cm-thick disks by a hot extraction method [21]. The conditions of the experiment are shown in Table 6.

For the given initial experimental conditions, the sample contains both an α-Zr region and a two-phase (α + δ)-Zr region (Fig. 8). This occurs because the initial concentration of 130 ppm by weight (1.16 at.% H) cuts the *α-Zr* terminal solubility line, N_α, (given by Sawatzky and Vogt [22]) at around $T_0 = 590$ K). This initial interface temperature corresponds to a distance of 1.34 cm into the sample as a result of a linear temperature gradient with slope *K*. The diffusion of hydrogen is only considered along the length of the sample (*x* direction) and this one-dimensional model is outlined in Fig. 8, with cornerstone equations and constants used in the model shown in Tables 7 and 8, respectively. In the derived model, N_1 is the hydrogen concentration in the single-phase α-Zr region, N_2 is the total hydrogen concentration in the two-phase (α + δ)-Zr mixture region, which is the sum of hydrogen in the saturated α-Zr portion of the phase and that in the δ-hydride portion of the mixture. In addition, N_δ is the δ-hydride saturation line, *J* is the hydrogen flux with respect to the fixed boundary at $x = 0$ in Fig. 8, v is the moving-boundary interface velocity and *D* is the hydrogen diffusion coefficient. Following the model of Sawatzky and Vogt, A_α and A_δ are the fractional areas occupied by each component at a cross section normal to the flux, where the areas are taken as equal to the relative amounts of α- and δ-phases present at each temperature based on the assumption that the densities of the α and δ phases are equal. At the moving boundary, the hydrogen concentration is fixed at the terminable solubility N_α with a continuity of flux into the two-phase region in Fig. 8.

The boundary conditions for the model are also outlined in Fig. 8. The Zircaloy-2 samples used in the experiment were covered with a ZrO_2 layer that acted as an insulator to hydrogen transport. Thus, the boundary conditions at the inner and outer surfaces of the specimen are normally taken as a zero flux in the experiment simulation [24]. Therefore, the boundary condition at $x = 2.50$ cm is treated as a reflexive Neumann condition. However, in the current analysis at $x = 0$ cm, in the $\alpha + \delta$ region, this boundary value is pinned to the experimental value at the data point *b*. The reasoning for using this less general and more restrictive condition is twofold: (i) no boundary with zero flux can exist for a two-phase

Table 6
Experiment conditions used in analytical modelling of [22] and the COMSOL model.

Length of Zircaloy-2 sample	2.5 cm
Diameter of Zircaloy-2 sample	1.2 cm
Initial homogenous hydrogen concentration N^o	130 ppm by weight
Temperature at cold end of sample T_{Cold}	403 ± 3 K
Temperature at hot end of sample T_{Hot}	750 ± 3 K
Linear temperature gradient *K*	138.8 ± 2.4 K cm^{-1}
Redistribution time in temperature gradient	34 d

Table 7
Cornerstone equations for the kinetics model.

Single-phase α-Zr

$\frac{dN_1}{dt} = -\nabla \cdot J_\alpha$

$J_\alpha(x) = -D_\alpha(T)(\nabla N_1(x) + \frac{Q^*_\alpha N_1(x)}{RT^2}\nabla T(x))$

$D_\alpha(T) = D^0_\alpha e^{-Q_\alpha/RT}$, $K = \nabla T(x) = \frac{dT}{dx}$

Two-phase (α + δ)-Zr

$\frac{dN_2}{dt} = -\nabla \cdot J_{\alpha+\delta}$

$J_{\alpha+\delta} = J^S_\alpha A_\alpha + J_\delta A_\delta$, $A_\alpha = \frac{N_\delta - N_2}{N_\delta - N_\alpha}$, $A_\delta = \frac{N_2 - N_\alpha}{N_\delta - N_\alpha}$

$J^S_\alpha(x) = -D_\alpha(T)(\nabla N_\alpha(x) + \frac{Q^*_\alpha N_\alpha(x)}{RT^2}\nabla T(x))$

$D_\alpha(T) = D^0_\alpha e^{-Q_\alpha/RT}$, $N_\alpha = N^0_\alpha e^{-\Delta H/RT}$, $K = \nabla T(x) = \frac{dT}{dx}$

$J_\delta(x) = -D_\delta(T)(\nabla N_\delta(x) + \frac{Q^*_\delta N_\delta(x)}{RT^2}\nabla T(x))$

$D_\delta = D^0_\delta e^{-Q_\delta/RT}$, $K = \nabla T(x) = \frac{dT}{dx}$

Moving boundary α/α + δ interface

$v = \frac{J_{\alpha+\delta} - J_\alpha}{(N_2 - N_\alpha)}$

Temperature

$T(x) = T(0) + Kx$, T(0) = 403 K

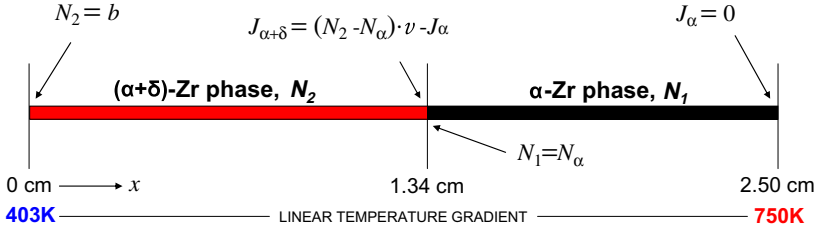

Fig. 8. Sawatzky and Vogt experiment simulation with boundary conditions at $t = 0$ and $N^0 = 130$ ppm by weight.

Table 8
Constants used in numerical model.

Symbol	COMSOL name	Definition	Value
D_α^0	Dalpha0	α phase frequency factor	1.09×10^{-3} cm^2 s^{-1}
D_δ^0	Ddelta0	δ phase frequency factor	1.09×10^{-3} cm^2 s^{-1}
ΔH	H	α phase heat of mixing	31,760 J mol^{-1}
K	K	Linear temperature gradient	138.8 K cm^{-1}
N^0	intN	Initial hydrogen concentration	130 ppm by weight
N_α^0	Nalpha0	α phase saturation constant	85,000 ppm by weight
N_δ	Ndelta	δ-hydride saturation line	16,000 ppm by weight
Q_α	Qalpha	α phase activation energy	34,670 J mol^{-1}
Q_α^*	Qalphastar	α phase heat of transport	25,070 J mol^{-1}
Q_δ	Qdelta	δ phase activation energy	47,640 J mol^{-1}
Q_δ^*	Qdeltastar	δ phase heat of transport	5430 J mol^{-1}
R	R	Universal gas constant	8.3145 J K^{-1} mol^{-1}
B	B	Experimental data point	192 ppm by weight

region, and (ii) a two-phase region will not exist at the boundary of the sample but instead a single-phase region of δ-hydride should be present [22]. However, since the given concentration is insufficient to cause precipitation of this phase and the boundary is at the cold end where hydrogen diffusion is slow, a simple approach was used instead to just fix the concentration at the experimental value of b (Table 8) [21].

For the moving interface, a moving mesh was applied using an Arbitrary Lagrangian–Eulerian (ALE) formulation [26] where the internal boundary (interface) moved with a velocity v (see Table 7). At the moving boundary for the α-Zr phase, a Dirichlet condition is chosen with the hydrogen concentration fixed at the terminal solubility, N_α. This arises from the definition of the terminal solubility where N_α is the minimum hydrogen concentration required to form δ-hydride. This value is specifically the initiation step for the formation of the two-phase $\alpha + \delta$ region. The boundary condition at the interface in Fig. 8 for the δ-hydride region is input as a continuity of flux at the interface.

The COMSOL simulation for the experiment for 34 d is shown in Fig. 9 with respect to the experimental data of Ref. [21] and the analytical solution of Ref. [22]. Fig. 9 confirms that the numerical solution is consistent with both the experimental data and the analytical solution of Sawatzky and Vogt. The numerical solution is sensitive to both the diffusion coefficient of hydrogen in α-Zr and the thermodynamic constants used to define the terminal solubility of α-Zr ($\alpha/\alpha + \delta$ phase boundary). Table 9 shows the terminal solubility line represented by constants determined by the Zr–H model and those given by Sawatzky and Vogt. When the constants of the current Zr–H model are used, the α phase frequency factor, D_α^0, can be re-fit to match the experimental data. The result of this fit is shown in Fig. 9. Therefore, when the terminal solubility line from the Zr–H thermodynamic model is used, the diffusion coefficient matches the experimental data when $D_\alpha^0 = 1.63 \times 10^{-3}$ cm^2 s^{-1}.

In the Swatzky experiment, the given concentrations are insufficient to give rise to a pure δ-hydride phase. However, as discussed in Section 1, such hydride precipitation can give rise to massive hydriding leading to the so-called "sunburst" effect observed in defective fuel elements as shown in Fig. 1. The massive hydriding will occur as a result of hydrogen migration arising from both concentration-gradient and temperature-gradient (i.e., Soret effect) effects (see Table 7). However, as observed with controlled in-reactor experiments, once massive hydriding results, this localized area can attract further hydride with continued irradiation despite the

Table 9
Constants for the solubility line and associated frequency factor for α-Zr for the experiment fitting.

Terminal solubility model	Solubility constants: $N_\alpha = N_\alpha^0 e^{-\Delta H/RT}$		D_α^0 to best fit experimental data (cm^2 s^{-1})
	N_α^0 (ppm by weight)	ΔH (J mol^{-1})	
Zr–H thermodynamic model constants	103,050	4115	1.63×10^{-3}
Sawatzky and Vogt constants	85,000	3820	1.09×10^{-3}

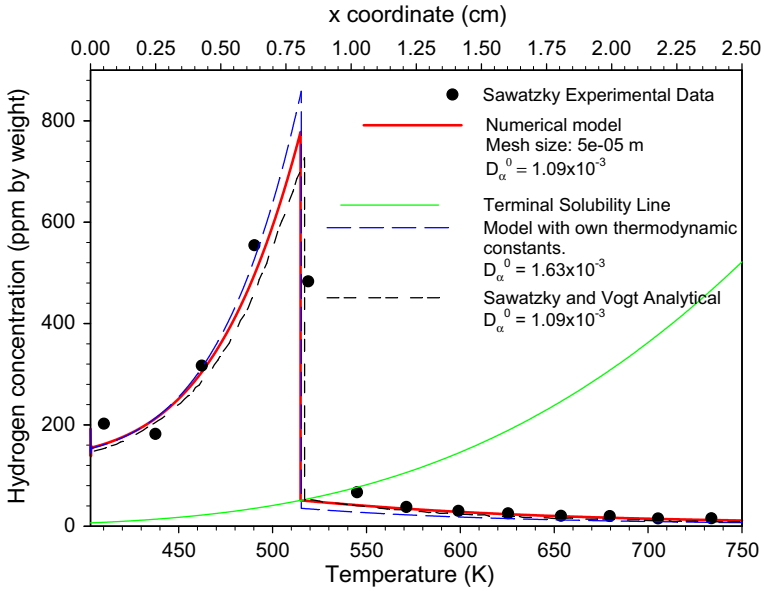

Fig. 9. COMSOL model numerical solution.

fact that a critical H_2/H_2O ratio is no longer present in the fuel-to-sheath gap [9]. The secondary hydride can grow due to the presence of a stress gradient field, which arises from the increased molar volume of the δ-hydride phase. In this case, the hydrogen mass flux equation in Table 7 must be modified with the addition of a driving force to account for hydrogen redistribution due to a stress gradient [25,27]:

$$J = -D\left(\nabla N + \frac{Q^* N}{RT^2}\nabla T - \frac{VN}{RT}\nabla\sigma\right) \quad (3)$$

Here J is the hydrogen flux ($\mathrm{mol\,m^{-2}\,s^{-1}}$), N is the hydrogen mass concentration ($\mathrm{mol\,m^{-3}}$), Q^* is the heat of transport due to diffusion ($\mathrm{J\,mol^{-1}}$), σ is the average normal stress (in the three principle directions) and V is the volume transport due to diffusion ($\mathrm{m^3\,mol^{-1}}$). However, in the Sawatzky hydride redistribution experiment, stress is not an important consideration because the hydrogen concentration is insufficient for a pure δ-hydride phase to form.

In summary, this work was carried out to provide a better understanding of hydriding phenomena leading to the proposal of a mitigation strategy for secondary hydriding now actively being pursued [11].

4. Conclusions

1. Thermodynamic models of the Zr–H and Zr–O–H systems have been developed. This treatment provides a calculation of the terminal solubility and partial pressure concentrations required to form hydride in the sheath. This analysis indicates that virtually pure H_2 is required to produce secondary hydride.
2. A kinetic model based on a finite-element analysis using the COMSOL multiphysics platform has been developed to describe hydrogen redistribution under a concentration and temperature gradient. The model has been benchmarked against the Sawatzky and Vogt experiment. This work provides a confirmation of the hydrogen diffusion coefficient in α-Zr.

Acknowledgements

The authors thank Atomic Energy of Canada Limited-Chalk River Laboratories for helpful discussions. The authors would also like to acknowledgement the CANDU Owners Group (COG) and University Network of Excellence in Nuclear Engineering (UNENE) for funding.

References

[1] J.M. Markowitz, Internal Zirconium Hydride Formation in Zircaloy Fuel Element Cladding Under Irradiation, WAPD-TM-351, Bettis Atomic Power Laboratory, May 1963.
[2] D.H. Locke, Nucl. Eng. Int. (August) (1969) 648.
[3] D.H. Locke, Nucl. Eng. Des. 21 (1972) 318–330.
[4] R.A. Proebstle, J.H. Davies, T.C. Rowland, D.R. Rutkin, J.S. Armijo, The mechanism of defection of zircaloy–clad fuel rods by internal hydriding, in: Proc. Topl. Mtg. Commercial Nuclear Fuel Technology Today, American Nuclear Society, Toronto, Canada, April 28–30, 1975.
[5] J.H. Davies, Secondary damage in LWR fuel following PCI defection – characteristics and mechanisms, in: Proc. Topl. Mtg. Defected Zirconium Alloy Clad Ceramic Fuel in Water Cooled Reactors, Chalk River, Canada, September 17–21, 1979, IWGFPT/6, p. 135, International Atomic Energy Agency 1980.
[6] B. Cox, Mechanisms of Hydrogen Absorption by Zirconium Alloys, AECL-8702, Atomic Energy of Canada Limited, November, 1984.
[7] J.C. Clayton, Internal Hydriding in Irradiated Defected Zircaloy Fuel Rods, in: Proc. 8th Int. Symp. Zirconium in the Nuclear Industry, STP 1023, American Society for Testing and Materials, 1989, p. 266.
[8] J.H. Davies and G.A. Potts, Post-defect behaviour of barrier fuel, in: Proc. Int. Topl. Mtg. LWR Fuel Performance, American Nuclear Society, Avignon, France, April 21–24, 1991, p. 272.
[9] B.J. Lewis, R.D. MacDonald, N.V. Ivanoff, F.C. Iglesias, Nucl. Technol. 103 (1993) 220.
[10] E. Yu Afanasieva, I.A. Evdokimov, V.V. Likhanskii, A.A. Sorokin, O.V. Khorizhii, V.V. Nivikov, Atom. Energy 95 (4) (2003) 689–695.
[11] G. Bruni, Framework for Sheath Hydriding Model for Defective Nuclear Fuel, MASc Dissertation, Royal Military College of Canada, May 2010.
[12] E. Zuzek, J.P. Abriata, A. San Martin, F.D. Manchester, Bull. Alloy Phase Diag. 11 (4) (1990) 386.
[13] D.R. Olander, General Thermodynamics, CRC Press, Boca Raton, FL, 2008.
[14] J.P. Abriata, J. Garces, R. Versaci, Bulle. Alloy Phase Diag. 7 (2) (1986) 388.
[15] G. Bruni, F∗A∗C∗T Final Project: Framework for Modelling Zr–H Binary System, Project in Fulfillment of the Course CC 519: Thermodynamic Computations in Materials Engineering, January 2009.
[16] R.F. Boyle, T.J. Kisiel, Hydrogen Permeation of Zircaloy-2 Corrosion Films, US Report, Bettis, Tech Rev., WAPD-BT-10, 1958, p. 31.
[17] D.W. Shannon, Role of Oxidation Rate on the Hydriding of Zirconium Alloys in Gas Atmospheres Containing Hydrogen, Corrosion, 19, 414t, and US Report HW-76562 REV, February 1963.
[18] R.L. Gibby, Hydriding of PRTR Fuel Rod End Caps, BNWL150 1965.
[19] Y. Kim, W. Wang, D.R. Olander, S.K. Yahnik, J. Nucl. Mater. 246 (1997) 43–52.
[20] O. Ohtaka, H. Fukui, K. Funakoshi, W. Utsumi, T. Irifune, T. Kikegawa, High Press. Res. 22 (2001) 221–226.
[21] A. Sawatzky, J. Nucl. Mater. (4) (1960) 321–328.
[22] A. Sawatzky, E. Vogt, Mathematics of Thermal Diffusion of Hydrogen in Zircaloy-2, Atomic Energy of Canada, AECL-1411, Chalk River, Ontario, October 1971.
[23] A. Sawatzky, E. Vogt, Trans. Met. Soc. AIME 227 (1963) 917.
[24] G.P. Marino, Nucl. Sci. Des. 49 (1972) 93–98.
[25] L. Lai, Z. Xu, Q. Jiang, A Method to Model Hydrogen Precipitation, in: 11th Proc. Int. Conf. Candu Fuel, Niagara Falls, Ontario, Canada, Canadian Nuclear Society, October 17–20, 2010.
[26] J. Donea, Antonio Huerta, J.-Ph. Ponthot, A. Rodriguez-Ferran, Arbritary Lagrangian–Eulerian methods, in: E. Stein, R. de Borst, T.J.R. Hughes (Eds.), Fundamentals of Encyclopedia of Computational Mechanics, vol. 1, Wiley& Sons, 2004. Chapter 14.
[27] P.G. Shewmom, Diffusion in Solid, McGraw-Hill, New York, 1963.